Cluster-Associated Filling of Water in Hydrophobic Carbon Micropores

Takako Kimura,[†] Hirofumi Kanoh,*[,†] Tomomichi Kanda,[†] Takahiro Ohkubo,[†] Yoshiyuki Hattori,[‡] Yasuyuki Higaonna,[†] Renaud Denoyel,[§] and Katsumi Kaneko[†]

Department of Chemistry, Faculty of Science, Chiba University, Chiba, 263-8522 Japan, Kashiwa Laboratory, Institute of Research and Innovation, 1201 Takada, Kashiwa, 277-0861 Japan, and Madirel, Unité mixte CNRS−Université de Provence, 26 rue du 141 RIA, 13003 Marseille, France

Received: March 9, 2004; In Final Form: July 6, 2004

The pore-wall chemistry of activated carbon fiber (ACF) was controlled by heating in Ar and H_2. The ACF structures were characterized from various levels, and interaction of water vapor with the micropores of ACF was directly measured by calorimetry. Two kinds of pitch-based ACFs with different pore widths (w) (P5, $w = 0.7$ nm, and P20, $w = 1.0$ nm) were used. P20 was treated at 1273 K in a gas flow of Ar or H_2 for 1 h to modify its surface properties. Adsorption isotherms of water on the two ACFs at 303 K showed different features, which are possibly caused by the pore width difference. The surface modification by the heat treatment of P20 changed its pore structure, leading to different water adsorption behavior. The mechanisms of water adsorption and desorption can be discussed through the differential or integral heat of water adsorption or desorption. Water adsorbs on the functional groups located at the surface of P20 with an adsorption heat comparable to the heat of condensation at relatively low P/P_0, causing the cluster formation of water molecules. The removal of such functional groups by heat treatment decreases the adsorption heat at low pressure. The differential heat abruptly increases at filling in all cases, indicating a structural formation of water from a clustered form to a highly ordered form.

Introduction

Recently nanocarbons have attracted attentions because of their wide application fields as well as offering interesting scientific systems: Especially, single-walled carbon nanotubes (SWNT) have promising potential for sensor technology, electronic devices, energy storage, and medical technology.[1−4] The affinity of SWNT for water is particularly important for potential applications.[5] Only molecular simulations have been applied to the studies on interactions between SWNT and water[6,7] because the purity of SWNT is not so high as to obtain reliable experimental data. Graphite nanopores such as activated carbons are expected to show interfacial properties for water similar to those of carbon nanotubes. If pure samples of graphite nanopores are available and reliable experimental data are obtained for the interaction between the graphite nanopores and water, the experimental results should give insight to understand the interaction between SWNT and water. Recently, single-walled carbon nanohorn (SWNH) assemblies, analogous to SWNT, which were prepared by Iijima et al. without any catalysts,[8] have been shown to adsorb water with an adsorption hysteresis.[9]

Activated carbon fiber (ACF) is one such graphite microporous material, which has considerably uniform micropores compared with conventional granular activated carbon. The micropore walls of ACF are mainly composed of the basal planes of nano-order graphitic units, providing a neutral and hydrophobic slit-shaped space whose width is on the order of 1 nm. The interaction of a neutral molecule with the graphitic micropore (pore width $w < 2$ nm) can be approximated by the sum of Steele's 10-4-3 potentials for the opposite pore walls,[10] leading to a deep potential well for micropores of $w < 1.5\sigma_{ff}$ (here σ_{ff} is the Lennard-Jones size parameter of the molecule). Then the adsorption of such vapor molecules begins from an extremely low relative pressure P/P_0; nitrogen adsorption in carbon micropores at 77 K must be measured from $P/P_0 = 10^{-6} \sim 10^{-5}$ at least in order to understand the adsorption mechanism. Organic vapors also can be adsorbed in carbon micropores from an extremely low P/P_0. However, a water molecule does not interact strongly with the graphitic slit pore. The characteristics of the water adsorption isotherm on a nonoxidized microporous carbon is a sigmoid form; the adsorption below $P/P_0 = 10^{-1}$ is negligible and the marked adsorption uptake starts near $P/P_0 = 0.5$ to fill micropores. This unique adsorption behavior has gathered much attention.[11] The difference from the typical capillary condensation was pointed out by McBain et al.[12] and Dubinin et al.[13] about 50−70 years ago, providing the cluster-associated adsorption mechanism without any structural evidence. Calorimetric studies on water adsorption on activated carbon were already done by them. The hydrophobic interaction had been an unsolved important subject although a number of experimental,[14] theoretical,[15] and computer simulation[16] studies were carried out. However, Ohba et al.[17] have solved this unclear problem quite recently: that is, cluster-associated adsorption and uniform desorption from condensed phase of water are developed in nanopores of ACF. The cluster formation makes water molecules less hydrophilic because dipole−dipole interaction between water molecules reduces the dipole moment of the cluster as a whole. This reduction of hydrophilicity leads to higher affinity of water cluster for hydrophobic graphitic walls and induces further ordering of water molecules at filling.

Such ordered structures of water molecules have been observed before. Iiyama et al.[18] determined the structures of

* Corresponding author: e-mail kanoh@pchem2.s.chiba-u.ac.jp.
[†] Chiba University.
[‡] Kashiwa Laboratory, Institute of Research and Innovation.
[§] Université de Provence.

10.1021/jp048934n CCC: $27.50
Published on Web 08/24/2004

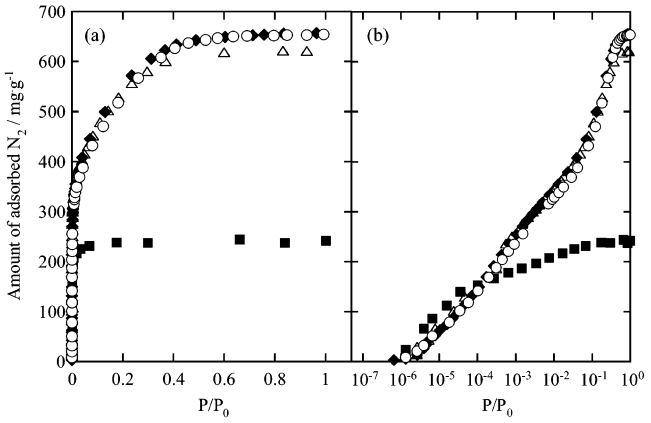

Figure 1. N_2 adsorption isotherms of P5 (■), P20 (◆), P20Ar (△), and P20H (○) at 77 K.

water adsorbed in micropores of ACF over the wide temperature range of 150−303 K. They showed that water confined in 0.8 nm pores at 303 K has a highly ordered structure that does not change, even at 150 K. They also examined the change of a small-angle X-ray scattering (SAXS) profile with adsorption and desorption, indicating the presence of different molecular association states upon adsorption and desorption.[19]

In this study, the pore-wall chemistry of ACF is controlled by heating in Ar and H_2, the ACF structures are characterized from different levels, and interaction of water vapor with the micropores of ACF is directly measured by calorimetry.

Experimental Section

Two kinds of pitch-based ACFs (P5 and P20, Ad'all Co.) were used. P5 and P20 were produced by different activation times. P20 was treated in an Ar or H_2 stream of 50 mL/min for 1 h at 1273 K. The treated P20 samples will be denoted P20Ar and P20H, respectively. The surface chemical structures of ACF samples were examined by X-ray photoelectron spectroscopy. The changes in the peak intensities of O1s and C1s with Ar etching time were examined. The oxygen content in the bulk pore wall was determined at the etching time of 5 min. The high-resolution N_2 adsorption isotherms of ACF samples were determined at 77 K gravimetrically.

The water adsorption isotherms of ACF samples were measured at 303 K gravimetrically. ACF samples were evacuated at 383 K and 1 mPa for 1 h prior to adsorption measurements. The heat of adsorption of water on ACF samples at 303 K was measured with a twin-type microcalorimeter (Tokyo Riko Co., GAC-II). The differential and integral heats of adsorption of water were evaluated by use of a computer. The heat of desorption on P20Ar was also measured.

X-ray diffraction of P20, P20Ar, and P20H was measured at 303 K in vacuo by the transmission method with an angle-dispersive diffractometer (MXP3 system, MAC science). The monochromatic Mo Kα ($\lambda = 7.093 \times 10^{-2}$ nm) at 50 kV and 30 mA was used for the diffraction measurement. The temperature dependence of magnetic susceptibility of P20, P20Ar, and P20H was measured with a superconducting quantum interference device (SQUID; Quantum Design, MPMS5S) over the temperature range 1.8−300 K in vacuo.

Results and Discussion

1. Microporosity and Chemical Structure of ACFs. Figure 1 shows the high-resolution N_2 adsorption isotherms of P5, P20, P20Ar, and P20H at 77 K. The adsorption isotherm of P5 is of representative type I (Figure 1a) and adsorption at low-pressure range is greater than that of P20 (Figure 1b), indicating that the micropore width of P5 is smaller than that of P20. The treatment of ACF in H_2 at 1273 K did not change the adsorption isotherm of P20. Hence, the microporosity of P20H should be almost the same as that of P20. Heat treatment of P20 in Ar at 1273 K decreased the amount of adsorption by 8%. Evolution of a slight amount of surface functional groups of P20 during the heat treatment in Ar probably changes the micropore structure. High-resolution α_s and DR analyses were applied to these N_2 adsorption isotherms.[20] Chemical compositions of the surfaces of the materials were analyzed by X-ray photoelectron spectroscopy (XPS). These results were tabulated in Table 1.

TABLE 1: Micropore Structures, O/C Mole Ratios, and Effective Spin Concentrations of ACFs[a]

samples	v_m (mL·g^{-1})	a_s (m^2·g^{-1})	w (nm)	O/C	n_{eff} (10^{-19} spins·g^{-1})
P5	0.29	906	0.7	0.095	1.3
P20	0.78	1530	1.0	0.123	2.8
P20Ar	0.78	1520	1.0	0.092	2.0
P20H	0.80	1470	1.1	0.043	1.6

[a] v_m, micropore volume; a_s, specific surface area; w, pore width; n_{eff}, effective spin concentration.

The surface area of P5 is much smaller than that of P20. The average pore width w of P5 is 0.7 nm, while w of P20 is 1.0 nm. Both treatments in Ar and H_2 do not seriously change the w value. Accordingly, it is clear that P20Ar and P20H are appropriate ACF samples for examination of the effect of surface chemistry on water adsorption.

The surface oxygen content was determined by XPS measurement. The species of surface oxygen groups was determined from the tail of C1s peak by an established deconvolution method. Analysis of the C1s peak of P20Ar showed only a slight decrease in surface functional groups from that of the pristine P20. It is because P20Ar was exposed to air after the heat treatment in Ar and then a portion of the surface carbon atoms could be reoxidized. On the contrary, the surface oxygen in P20H is less compared with that of P20Ar. Thus, heat treatment in H_2 stabilizes nanographitic structures even in an atmospheric environment. The dangling bonds in P20 can react with H_2 to form C−H bond by the high-temperature treatment in H_2, while the Ar treatment removes the surface functional groups and produces the active carbon sites, which are then reoxidized upon exposure to air after the Ar treatment. This difference is evidenced by the SQUID measurements as shown below.

The change in the dangling bond with heat treatment was examined by magnetic susceptibility (χ) measurements at low temperature. χ increases with the decrease in temperature at low-temperature range, as shown in Figure 2. The χ value for P20Ar and P20H is negative near 300 K, indicating the diamagnetism that stems from the nanographitic structure.[21] The effective spin density n_{eff} was determined from the Curie−Weiss plot. n_{eff} values are also listed in Table 1. Their order is P20 > P20Ar > P20H. Hence, P20H should be the most stable, because the carbon atom of the dangling bond is terminated by an H atom. This result coincides with the XPS results mentioned above.

2. Water Adsorption of ACFs. Figure 3 shows adsorption isotherms of water on P5 and P20 at 303 K. The ordinate is normalized by use of the maximum amount of water adsorption near $P/P_0 = 1$ and represented as fractional filling ϕ. The two isotherms completely differ from each other. The adsorption of water on P5 begins at $P/P_0 < 0.1$; the amount of water adsorption increases linearly with P/P_0 until $P/P_0 = 0.25$ and rises at around $P/P_0 = 0.3$, followed by a gradual increase at $P/P_0 > 0.45$. The adsorption isotherm of P5 does not show

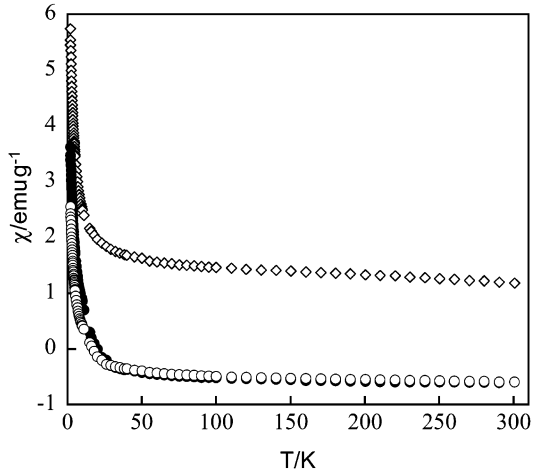

Figure 2. Temperature dependence of magnetic susceptibilities of P20 (◇), P20Ar (●), and P20H (○).

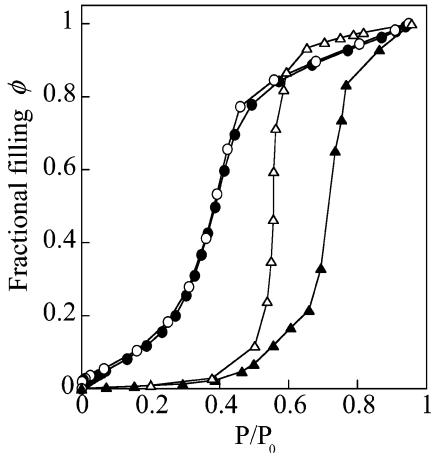

Figure 3. Water adsorption isotherms of P5 (●, ○) and P20 (▲, △) at 303 K. Solid and open symbols denote adsorption and desorption branches, respectively.

adsorption hysteresis, whereas the adsorption of water on P20 proceeds little until $P/P_0 = 0.40$. An abrupt increase in adsorption amount is observed at about $P/P_0 = 0.7$. The desorption branch does not overlap with the adsorption one, giving a representative adsorption hysteresis. As an explicit difference between P5 and P20 is only in the pore width, this marked variation between the adsorption isotherms must be attributed to the pore width difference. This is a noteworthy effect.

Figure 4 shows the change in the adsorption isotherm of water on P20 with high-temperature treatment. The heat treatment in Ar shifts the rising branch of adsorption to the higher P/P_0 without changing the desorption branch, while the heat treatment in H_2 shifts both branches of adsorption and desorption to the higher P/P_0, although the effect is less than that in Ar. Heat treatment in H_2 decreases the amount of water adsorption below $P/P_0 = 0.2$, and the rising curve near 0.7 becomes sharper by the H_2 treatment. This can be due to a decrease in oxygenated surface groups.

3. Heat of Water Adsorption. Figure 5 shows the differential heat q_d of water adsorption against P/P_0 for P5 and P20. The water adsorption isotherms are shown in each figure for comparison. Also, the heat q_{cond}, corresponding to the heat of condensation of water vapor (45.05 kJ mol^{-1}), $q_{cond} = 45.05 - RT$, is shown by a broken line. The q_d of water adsorption for P5 increases gradually from 16 to 80 kJ·mol^{-1} and then

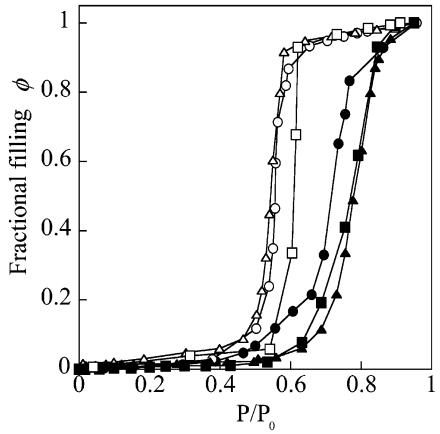

Figure 4. Water adsorption isotherms of P20 (●, ○), P20Ar (▲, △), and P20H (■, □) at 303 K. Solid and open symbols denote adsorption and desorption branches, respectively.

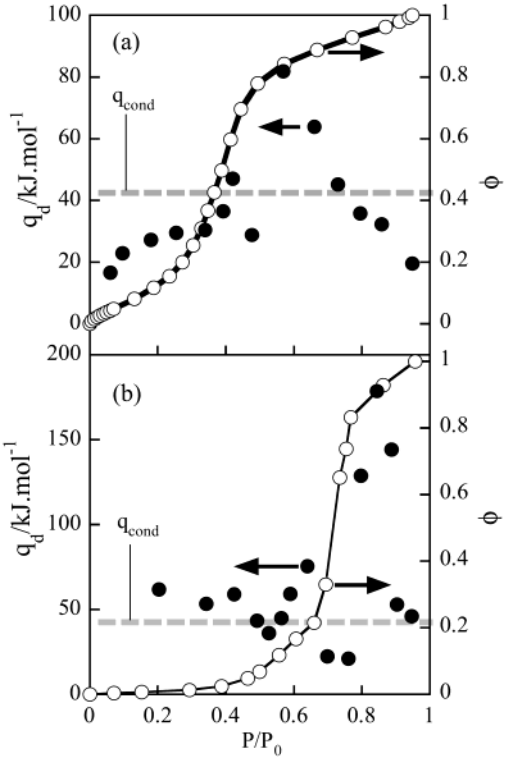

Figure 5. Differential heat (q_d, ●) of water adsorption on P5 (a) and P20 (b). Fractional filling (ϕ, ○) is also shown. Broken lines denote the heat of condensation of water (q_{cond}).

decreases to 20 kJ·mol^{-1} as P/P_0 increases. The region having a greater q_d than the heat of condensation (q_{cond}) corresponds to the abrupt uptake in the presaturation. Hence, the large q_d should be associated with the prefilling process of water in narrow micropores. The q_d vs P/P_0 profile for P20 is different from that of P5. Almost all observed q_d values in the whole range are greater than q_{cond}. In this case, surface functional groups should raise the q_d value. The q_d value steeply increases with P/P_0, in parallel to the adsorption isotherm, and then drops near $P/P_0 = 0.9$. Although the steep increase in q_d near the abrupt water uptake is similar to that observed in P5, the absolute top value of q_d for P20 is remarkably high (~150 kJ·mol^{-1}), suggesting the possibility of not only stabilization of adsorbed water but also its change to a more highly ordered structure.

The integral heat q_i of water adsorption provides a different aspect, as shown in Figure 6. The q_i values on the whole range

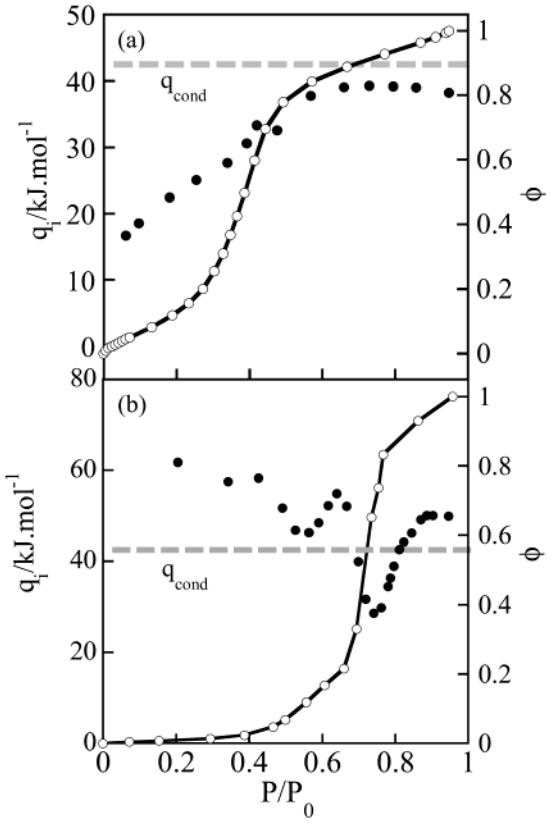

Figure 6. Integral heat (q_i, ●) of water adsorption on P5 (a) and P20 (b). Fractional filling (ϕ, ○) is also shown. Broken lines denote the heat of condensation of water (q_{cond}).

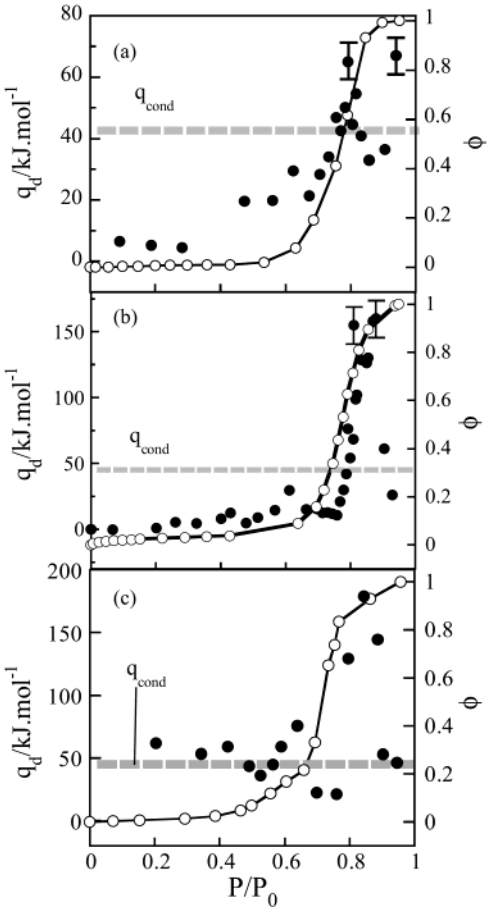

Figure 7. Differential heat (q_d, ●) of water adsorption on P20H (a), P20Ar (b), and P20 (c). Fractional filling (ϕ, ○) is also shown. Broken lines denote the heat of condensation of water (q_{cond}).

are situated below q_{cond} in the case of P5, whereas P20 has a unique variation: q_i at $\phi < 0.65$ and $\phi > 0.85$ is greater than q_{cond}. Accordingly, micropores of P5 are not favorable for formation of bulk liquid structure. An in situ X-ray diffraction study showed that water in micropores of P5 has a highly ordered structure compared with the bulk liquid (not shown). Such an ordered state of water in micropores of P5 is not necessarily stable in comparison with the bulk liquid state. In case of P20, q_i at the initial stage of adsorption should stem from the excess interaction of a water molecule with the surface functional group through the permanent dipole−local electric field on the surface functional group. The greater q_i value at $\phi = 0.2$ may be ascribed to stabilization by the preadsorbed water clusters on the surface functional groups. Another high q_i region near $\phi = 1$ should originate from additional stabilization other than that for the adsorbed molecular assembly. Also, the preceding X-ray diffraction study showed that the structure of water confined in micropores of P20 is much less ordered than that of P5.[18]

4. Effect of Surface Chemistry on Heat of Adsorption. Figure 7 shows plots of q_d and ϕ vs P/P_0 for P20, P20Ar, and P20H. The q_d profile of P20 is quite different from those of P20Ar and P20H at low P/P_0 region. This difference is associated with removal of the surface functional groups. The steep rise at filling at $0.75 < \phi < 0.85$ is common for all three samples. This should be caused by the stabilization of adsorbed water in micropores. Thus, the filling of water molecules in hydrophobic micropores occurs irrespective of the presence of the surface functional groups. From these results, it is unlikely that the mechanism which has long been recognized for the water adsorption−desorption on hydrophobic graphite nanopores is essential.

Figure 8 shows the changes of q_i of P20, P20Ar, and P20H. The three relationships are different from one another. The q_i value of P20H at filling is the smallest of the three samples and slightly smaller than q_{cond}, whereas the dependence of q_i and ϕ on P/P_0 for P20Ar almost overlaps and correlates with that for P20 at $\phi > 0.7$. These are probably related to the extent of removal of the surface functional groups. The assembly of water molecules in the pores of P20 and P20Ar is likely to be more stable than that of P20H because the q_i values for P20 and P20Ar near $P/P_0 = 1$ are greater than q_{cond}. Consequently, the final filling processes of micropores by water for P20 and P20Ar should be the same; the initial stages of adsorption are different, depending on the presence or almost absence of the surface functional groups on the micropore walls.

5. Heat of Desorption of Water. The heat of water desorption on P20Ar is shown in Figure 9. The heat is absorbed upon desorption, and then the negative value of the heat of desorption is used for comparison with the heat of adsorption. The values of $|q_d|$ for desorption at $0.7 < \phi < 0.9$ are comparable to q_{cond}, indicating an ordinary evaporation of molecules from the interface of an almost fully adsorbed layer in micropores. Thus, the $|q_d|$ value for desorption is quite different from that for adsorption, indicating that the desorption proceeds via a molecular assembly different from that in the adsorption process. The difference between the two processes is supported by the results of $|q_d|$ values. The $|q_d|$ drops from about 40 to 10 kJ·mol^{-1} at $\phi = 0.5$. After this critical desorption, $|q_d|$ becomes much lower than q_{cond}, indicating a weak interaction like that in the adsorption process at low ϕ, where an island structure of small water clusters is suggested.

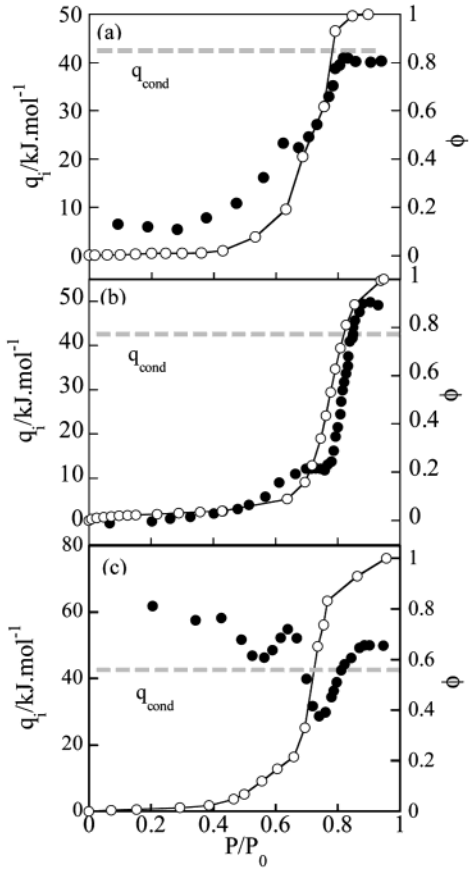

Figure 8. Integral heat (q_i, ●) of water adsorption on P20H (a), P20Ar (b), and P20 (c). Fractional filling (ϕ, ○) is also shown. Broken lines denote the heat of condensation of water (q_{cond}).

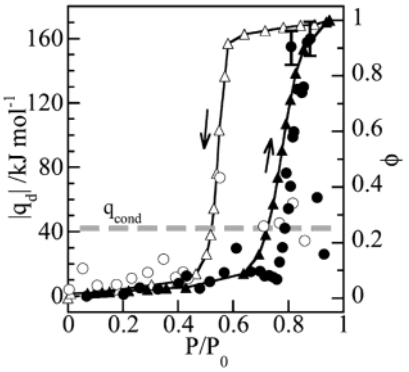

Figure 9. Differential heat ($|q_d|$) of water adsorption (●) and desorption (○) on P20Ar. Fractional filling (ϕ) for adsorption (▲) and desorption (△) are also shown. Broken lines denote the heat of condensation of water (q_{cond}).

6. Mechanism for Water Adsorption and Desorption in Hydrophobic Micropores. A single water molecule interacts very weakly with the graphite surface. The interaction energy should be comparable to or less than the thermal energy at ambient temperature. Then water molecules are not adsorbed on carbon micropores at the low pressure. If there is a low content of surface functional groups, water molecules are adsorbed on these sites to form small clusters. At some higher pressure, the growth of water clusters occurs and causes filling. This is an old model that has been believed for a long time.[11] However, similar adsorption appears for even microporous materials with a lower content of surface functional groups, as is shown in the present study.

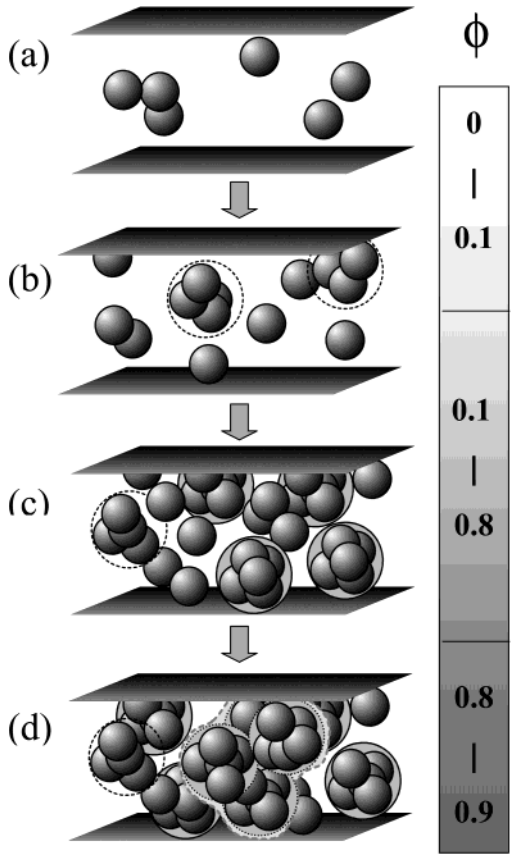

Figure 10. Mechanism of water adsorption: (a) association of water molecules, (b) cluster formation, (c) enhancement of interaction between clusters and walls, and (d) formation of highly ordered structures.

Ohba et al.[17] have quite recently shown that the clusterization of water molecules in the graphite nanopores (w = 1.1 nm) transforms the chemical affinity of water molecules from hydrophilicity to hydrophobicity.[17] A single water molecule interacts very weakly with the graphite slit pore. A water molecule can be stabilized by the molecule−molecule interaction in the cluster on cluster formation; the stabilization in the nanopores becomes greater with increasing cluster size (Figure 2 in ref 17). An association number of 8−10 is proposed for the optimum cluster size in the graphite nanopore. Thus, these lead to the following mechanism for water adsorption on graphite nanopores.

Water molecules are not adsorbed on the graphite nanopores at low pressure, but a small amount of water molecules can be inserted into the pores because of the slight molecule−pore wall interaction and/or less hydrophilicity of water molecules due to a partial dimerization in the gaseous phase, as shown in Figure 10a. Then, more water molecules are adsorbed on those confined in the nanopores and small clusters are formed with an increase in P/P_0 (Figure 10b). The enthalpy change for these processes is less than that for ordinary adsorption processes such as N_2 adsorption at 77 K. For a higher pressure range, the cluster grows with relatively low heat of adsorption until filling (Figure 10c). At filling, highly ordered structures are formed from several clusters with a great enthalpy change (Figure 10d). Simultaneously, the interaction between the carbon walls and water clusters is enhanced because of the affinity change due to clusterization. Thus, the heat of adsorption changes according to the mechanism. The marked high value of q_d (∼150 kJ mol^{-1}) originates from the accumulation of a series of enhancement effects and is not unlikely.

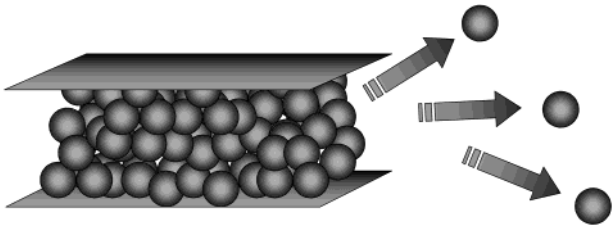

Figure 11. Mechanism of water desorption (continuous process).

In contrast, the heat of desorption is quite different because the desorption proceeds uniformly from a condensed state. This mechanism agrees with the density fluctuation changes of adsorbed water in pores on adsorption and desorption from in situ SAXS[19] and is also supported by the simulation study.[22] Thus, the desorption mechanism is based on a continuous process from uniform layers of water molecules. This feature is represented schematically in Figure 11. This suggests that the desorption process is closer to the thermodynamic equilibrium state than that for the adsorption process, which is in a metastable state. If equilibration time for an adsorption branch in experiments is long enough, a P/P_0 value at the uprise of adsorption will shift to the left. This can be checked partially.

Therefore, the present study has solved an important problem that had long been unsolved.

Acknowledgment. We acknowledge the Japan Society for the Promotion of Science (JSPS) for the Grant-in-Aid for Scientific Research (C) (15550171).

References and Notes

(1) Zhou, G.; Kawazoe, Y. *Chem. Phys. Lett.* **2001**, *350*, 386.
(2) Frackowiak, E.; Béguin, F. *Carbon* **2002**, *40*, 1775.
(3) Saito, Y.; Uemura, S. *Carbon* **2000**, *38*, 169.
(4) Gevorgian, L. A.; Ispirian, K. A.; Ispirian, R. K. *Nucl. Instrum. Methods Phys. Res. B* **1998**, *145*, 155.
(5) Hummer, G.; Rasaiah, J. C.; Noworyta, J. P. *Nature* **2001**, *414*, 188.
(6) Koga, K.; Gao, G. T.; Tanaka, H.; Zeng, X. C. *Nature* **2001**, *412*, 802.
(7) Walther, J. H.; Jaffe, R.; Halicioglu, T.; Koumoutsakos, P. *J. Phys. Chem. B* **2001**, *105*, 9980.
(8) Iijima, S.; Yudasaka, M.; Yamada, R.; Bandow, S.; Suenaga, K.; Kokai, F.; Takahashi, K. *Chem. Phys. Lett.* **1999**, *309*, 165.
(9) Bekyarova, E.; Hanzawa, Y.; Kaneko, K.; Silvestre-Albero, J.; Sepulveda-Escribano, A.; Rodriguez-Reinoso, F.; Kasuya, D.; Yudasaka, M.; Iijima, S. *Chem. Phys. Lett.* **2002**, *366*, 463.
(10) Steele, W. A. *Surf. Sci.* **1973**, *36*, 317.
(11) Mowla, D.; Do, D. D.; Kaneko, K. *Chem. Phys. Carbon* **2003**, *28*, 229.
(12) McBain, J. W.; Porter, J. L.; Sessions, R. F. *J. Am. Chem. Soc.* **1933**, *55*, 2294.
(13) Dubinin, M. M.; Zaverina, E. D.; Serpinsky, V. V. *J. Chem. Soc.* **1955**, 1760.
(14) (a) Brennan, J. K.; Bandosz, T. J.; Thomson, K. T.; Gubbins, K. E. *Colloid Surf. A* **2002**, *187*−*188*, 539−568. (b) Lodewyckx, P.; Vansant, E. F. *Carbon* **1999**, *37*, 1647. (c) Stoeckli, F.; Lavanchy, A. *Carbon* **2000**, *38*, 475. (d) Lodewyckx, P.; Van Rompaey, D.; Verhoeven, L.; Vansant, E. F. *Carbon* **2001**, *39*, 309. (e) Carrasco-Mari, F.; Mueden, A.; Centeno, T. A.; Stoeckli, F.; Moreno-Castilla, C. *J. Chem. Soc., Faraday Trans.* **1997**, *93*, 2211. (f) Salame, I. I.; Bandosz, T. J. *Langmuir* **1999,** *15*, 587−593. (g) Hanzawa, Y.; Kaneko K. *Langmuir* **1997**, *13*, 5802. (h) Salame, I. I.; Bagreev, A.; Bandosz, T. J. *J. Phys. Chem. B* **1999**, *103*, 3877−3884. (i) Salame, I. I.; Bandosz, T. J. *Langmuir* **2000**, *16*, 5435−5440.
(15) (a) Talu, O.; Meunier, F. *AIChE J.* **1996**, *42*, 809. (b) Do, D. D.; Do, H. D. *Carbon* **2000**, *38*, 767. (c) Slasli, A. M.; Jorge, M.; Stoeckli, F.; Seaton, N. A. *Carbon* **2003**, *41*, 479−486.
(16) (a) Müller, E. A.; Rull, L. F.; Vega, L. F.; Gubbins, K. E. *J. Phys. Chem.* **1996**, *100*, 1189. (b) McCallum, C. L.; Bandoz, T. J.; McGrother, S. C.; Müller, E. A.; Gubbins, K. E. *Langmuir* **1999**, *15*, 533. (c) Feller, D.; Jordan, K. D. *J. Phys. Chem. A* **2000**, *104*, 9971. (d) Gordillo, M. C.; Marti L, J. *J. Chem. Phys.* **2002**, *117*, 3425. Brennan, J. K.; Thomson, K. T.; Gubbins, K. E. *Langmuir* **2002**, *18*, 5438. (e) Jorge, M.; Schumacher, C.; Seaton, N. A. *Langmuir* **2002**, *18*, 9296. (f) Jorge, M.; Seaton, N. A. *Mol. Phys.* **2002**, *100*, 3803−3815. (g) Striolo, A.; Gubbins, K. E.; Chialvo, A. A.; Cummings, P. T. *Mol. Phys.* **2004**, *102*, 243−251. (h) Müller, E. A.; Hung, F. R.; Gubbins, K. E. *Langmuir* **2000**, *16*, 5418−5424.
(17) Ohba, T.; Kanoh, H.; Kaneko, K. *J. Am. Chem. Soc.* **2004**, *126*, 1560.
(18) Iiyama, T.; Nishikawa, K.; Suzuki, T.; Kaneko, K. *Chem. Phys. Lett.* **1997,** *274*, 152.
(19) Iiyama, T.; Ruike, M.; Kaneko, K. *Chem. Phys. Lett.* **2001,** *331*, 359.
(20) Kaneko, K. *J. Membr. Sci.* **1994,** *96*, 59.
(21) Kaneko, K.; Ishii, C.; Kanoh, H.; Hanzawa, Y.; Setoyama, N.; Suzuki, T. *Adv. Colloid Interface Sci.* **1998**, *76*−*77*, 295.
(22) Ohba, T.; Kanoh, H.; Kaneko, K. *J. Phys. Chem. B* **2004** (in press).